Journal of Nuclear Materials 400 (2010) 127–137

Contents lists available at ScienceDirect

Journal of Nuclear Materials

journal homepage: www.elsevier.com/locate/jnucmat

# Effect of pre-strain on creep of three AISI 316 austenitic stainless steels in relation to reheat cracking of weld-affected zones

Q. Auzoux [a,*], L. Allais [a], C. Caës [a], I. Monnet [a,1], A.F. Gourgues [b], A. Pineau [b]

[a] CEA, DEN, SRMA, Bat 455, 91191 Gif-sur-Yvette, France
[b] MINES ParisTech, Centre des Matériaux, CNRS UMR 7633, BP 87, 91003 Evry cedex, France

ARTICLE INFO

*Article history:*
Received 19 November 2009
Accepted 23 February 2010

ABSTRACT

Microstructural modifications induced by welding of 316 stainless steels and their effect on creep properties and relaxation crack propagation were examined. Cumulative strain due to multi-pass welding hardens the materials by increasing the dislocation density. Creep tests were conducted on three plates from different grades of 316 steel at 600 °C, with various carbon and nitrogen contents. These plates were tested both in the annealed condition and after warm rolling, which introduced pre-strain. It was found that the creep strain rate and ductility after warm rolling was reduced compared with the annealed condition. Moreover, all steels exhibited intergranular crack propagation during relaxation tests on Compact Tension specimens in the pre-strained state, but not in the annealed state. These results confirmed that the reheat cracking risk increases with both residual stress triaxiality and pre-strain. On the contrary, high solute content and strain-induced carbide precipitation, which are thought to increase reheat cracking risk of stabilised austenitic stainless steels did not appear as key parameters in reheat cracking of 316 stainless steels.



## 0. Introduction

Intergranular cracking can occur in heat-affected zones (HAZ) of austenitic stainless steel welded joints when reheated in the temperature range from 500 to 700 °C. In this temperature range, residual stresses due to welding relax by creep flow but the HAZ may not sustain this small strain if its microstructure has been too severely altered during welding. This type of cracking, called reheat cracking, was originally identified in the 1950s on Nb-stabilised austenitic stainless steel AISI 347 [1,2]. Younger et al. [3,4] showed that primary carbides can be dissolved during welding and may precipitate during service around 600 °C as fine intragranular secondary carbides, which nucleate at dislocations that are introduced by the welding process. This secondary precipitation was found to cause a substantial increase in hardness. It was thus suggested that the low ductility intergranular failures that occur in HAZ material at 600 °C, are caused by strain-induced precipitation hardening. As unstabilised austenitic stainless steels do not present primary carbides, they are less sensitive to reheat cracking [5], but recent occurrence of reheat cracking in 316H thick weldments [6–8] proved that they are not immune.

Following reheat cracking of AISI 321-welded components [9], Chabaud-Reytier et al. [10] studied the sensitivity of AISI 321 to reheat cracking. They first obtained simulated weld-affected zones by pre-straining and pre-ageing the material, then they measured their creep resistance and estimated their reheat-cracking sensitivity using a relaxation crack propagation test on Compact Tension (CT) specimens. Strain-induced precipitation caused by pre-ageing hardened the material at room temperature (as investigated with hardness measurements) but softened the material at 600 °C (i.e. their creep rate increased for a given stress). Moreover, reheat-cracking sensitivity was found to increase with increasing level of pre-strain and to decrease with level of pre-ageing. The authors attributed therefore the low ductility of the HAZ to intragranular hardening due to solute atoms–dislocations interactions rather than to dislocation–precipitate interactions. Such a mechanism is consistent with the reheat-cracking sensitivity of unstabilised stainless steels with a high solute content such as AISI 316H or 316L(N). It also suggests that AISI 316L would be less prone to cracking.

Recent work on reheat cracking of unstabilised austenitic stainless steels [11–17] mostly focused on the influence of stress triaxiality on intergranular damage and on the influence of pre-strain on creep ductility. However, these studies did not mention the role of solute atoms in the cracking mechanism. Three plates of AISI 316 stainless steels, containing different amounts of carbon and nitrogen (316H, 316L(N) and 316L) were therefore examined in the

* Corresponding author. Present address: CEA, DEN, SEMI, Bat 625P, 91191 Gif-sur-Yvette, France. Tel.: +33 1 69 08 18 34; fax: +33 1 69 08 93 24.
*E-mail address:* quentin.auzoux@cea.fr (Q. Auzoux).
[1] Present address: CEA, DSM, IRAMIS, CIRIL Caen, France.

0022-3115/$ - see front matter © 2010 Elsevier B.V. All rights reserved.
doi:10.1016/j.jnucmat.2010.02.021

present study. The objectives of this study were threefold: (i) estimation of the level of pre-strain in weld-affected zones, (ii) obtaining pre-strained materials representative of the most critical weld-affected zone, (iii) characterisation of these materials by both uniaxial creep testing on tensile specimens and relaxation testing on pre-cracked CT specimens.

## 1. Materials

The chemical composition of the three studied AISI 316 steels is reported in Table 1. The AISI 316H steel was received from British Energy. It was extracted from a 63-mm-thick reheat-cracked component after approximately 50,000 h at 500 °C [18]. Both parts including welds and parts away from welds were cut in order to examine reheat cracks, weld-affected zone, and base metal. 316L(N) and 316L were bought in the annealed state. In order to get unaged reference materials, a piece of the 316H base metal was annealed for 1 h at 1170 °C and argon gas cooled (~200 °C/min). Preliminary analysis revealed that the microstructure of the 316L(N) steel was not uniform. Therefore, it was annealed for half an hour at 1170 °C and argon gas cooled. The mean grain size after annealing treatments was 150 μm, 60 μm and 75 μm for 316H, 316L(N) and 316L, respectively. Half of the annealed plates were then warm-rolled between 400 °C and 600 °C to reduce their thickness by 15 ± 0.4% for 316L(N) and 316H and by 17.5 ± 0.4% for 316L. This temperature range and these values of thickness reduction ratio were chosen in order to reproduce the microstructure of the hardest area of the strain-affected zone of observed welds and to obtain similar hardness for all three pre-strained steels (see Section 3.2). Annealed and pre-strained materials were then subjected to mechanical testing described in Section 4.

## 2. Experimental procedures

The cylindrical smooth bars used for tensile and constant load creep tests on 316L and 316L(N) were cut perpendicularly to the rolling direction, those used for tests on 316H were cut parallel to the rolling direction. The gauge diameter was 4 mm and the gauge length was 20 mm. A capacitive transducer linked to the top and bottom ends of the specimens was used to measure strain during creep tests, whereas the load line displacement was used for tensile tests. The test temperature, controlled by three thermocouples attached to the specimen, was 600 ± 3 °C. Fracture elongation was determined from the last recorded point of the creep and tensile curves. Potential plastic elongation during creep test loading was included in the fracture elongation. Reduction of area at fracture was derived from laser diameter measurements made both before and after the tests.

CT specimens used for relaxation tests were 10 mm thick (side-grooved to 8 mm) and 40 mm wide. Concerning 316L and 316L(N), the load was applied transversally to the rolling direction, and the crack propagated along the rolling direction, whereas for 316H specimens, the load was applied along the rolling direction, and the crack propagated transversally to the rolling direction. The specimens were fatigue pre-cracked at room temperature up to $a_0/W = 0.50 \pm 0.01$ (with $a_0$ the length of the pre-crack and $W$ the distance between load line and rear side of the specimen). The opening displacement was monitored through a capacitive transducer with an accuracy of 0.5 μm. For all tests, the transducer was attached to the top and bottom of the specimen along the loading line. Relaxation crack growth tests were performed on an electro-mechanical machine. Pre-cracked CT specimens were first submitted to a constant loading rate (24 μm/min) and then to a constant opening displacement. After a given duration, the specimen was unloaded, then cooled down to room temperature and finally broken by fatigue crack propagation. Crack propagation during relaxation could then be measured on photographs of the fracture surface. The load values on CT specimens were converted into stress intensity factors using the ISO/DIS 12135 standard, which takes the side grooves into account.

In the samples extracted from in-service component, the chemical composition of the oxides filling the cracks was analysed on polished sections using a Cameca SX 50 electron probe microanalyser. Wavelength dispersive spectrometry profiles were taken across the cracks with a step size of 1 μm.

Broadening of X-ray diffraction peak of {3 1 1} planes due to the deformation induced by welding was recorded using an ELPHYSE Set-X type X-ray diffractometer with a manganese source operated under 20 kV. The angular step of the $2\theta$ scans was set to 0.09° with 60 s per step and the spot diameter was set to 3 mm. Prior to X-ray diffraction measurements, a surface layer of 275 μm in thickness was removed by electrolytic polishing in order to get free from machining-induced surface cold work. The peak width was evaluated as the area under the peak divided by its height and by a corrective factor of 1.5 that takes into account the fact that $K_{\alpha 1}$ and $K_{\alpha 2}$ peaks were not resolved.

Thin foils for TEM examinations on a Philips EM 430 microscope operated at 300 kV were cut at one quarter of the plate thickness and prepared by mechanical thinning down to 0.1 mm, followed by electrolytic thinning in a solution of 70% ethanol, 20% butoxyethanol and 10% perchloric acid, at 8 °C under 30 V. Bright field imaging, dark field imaging and micro-diffraction techniques were used to investigate dislocation microstructure and carbide precipitates.

## 3. Characterisation of weld-affected zones and pre-strained materials

### 3.1. Characterisation of weld-affected zones

#### 3.1.1. As-received 316H weld-affected zone

This section describes the characterisation of the reheat cracked weld-affected zone extracted after approximately 50,000 h at 500 °C. Intergranular cracks due to the coalescence of cavities (nucleated around intergranular particles) were observed in the weld-affected zone between 1 and 5 mm away from the fusion line. Some of the cracks were filled with oxide whereas some were not oxidized at all. A metallic filament enclosed by oxide was noticed in the middle of approximately half the length of the oxidized cracks. Electron probe microanalysis revealed that: (i) where no metallic filament was present, the central part of the cracks was occupied by iron oxide and the sides of the cracks by an iron-depleted oxide rich in chromium and nickel; (ii) where the metallic filament was present, it contained iron almost exclusively and was enclosed by larger layers of iron-depleted oxide rich in

**Table 1**
Chemical composition (weight %) of the three studied AISI 316 stainless steels (bal. Fe).

| Material | C | N | Cr | Ni | Mo | Mn | Si | Cu | S | P | Co | B |
|---|---|---|---|---|---|---|---|---|---|---|---|---|
| 316L(N) | 0.026 | 0.069 | 17.3 | 12.1 | 2.54 | 1.74 | 0.31 | 0.29 | 0.001 | 0.025 | 0.09 | 0.004 |
| 316H | 0.05 | 0.033 | 17.1 | 12 | 2.32 | 1.48 | 0.52 | – | 0.01 | 0.02 | 0.05 | 0.003 |
| 316L | 0.033 | 0.025 | 16.4 | 13.6 | 2.12 | 1.55 | 0.44 | <0.07 | 0.024 | 0.022 | 0.18 | 0.001 |

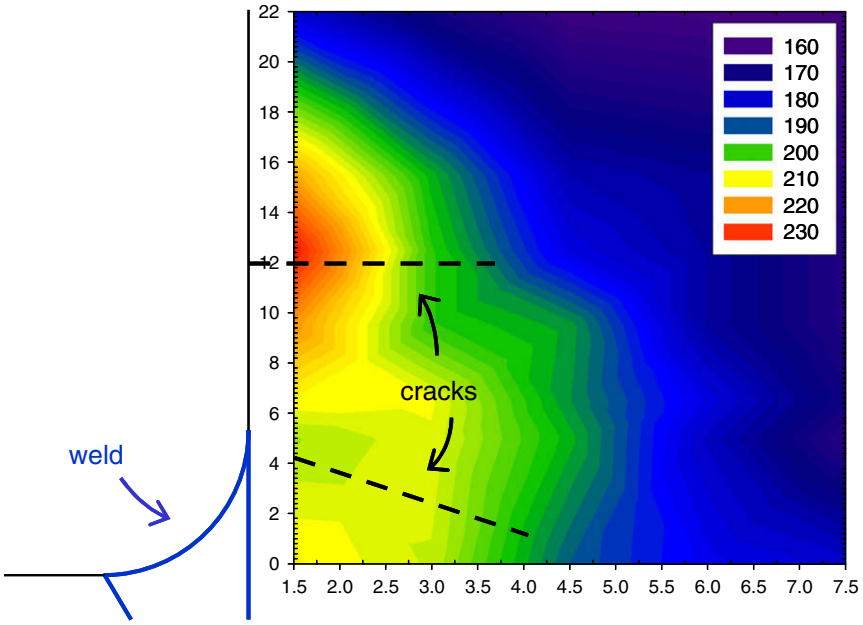


**Fig. 1.** Vickers hardness map (30 kg) around reheat cracks near an as-received weld of 316H steel, indicated dimensions are in millimetres.

chromium and nickel. The metallic iron filament could therefore result from the reduction of the iron oxide by the thermodynamically more stable chromium-rich oxide, when the local oxygen partial pressure decreased as a consequence of the crack being filled with oxide. These observations are in agreement with results reported in [8,19]. As cracks without oxide were also observed, oxidation was not considered as a cause for reheat cracking to occur but rather as a consequence of cracking. Relaxation crack propagation tests performed in vacuum also confirmed this interpretation [20].

As reported by Bouchard et al. [18], Vickers hardness measurements next to as-received 316H welds showed that cracks were located in a zone where hardness was higher than 200 $HV_{30}$ (Fig. 1). As described in [20] for unaged 316L(N) welds, Fig. 2 indicates that 316H weld-affected zone is much harder than the base metal. Fig. 3 shows that the weld-affected zone contains a very high dislocation density and more or less well-defined dislocation cells. Thin foils extracted at 20 mm away from the weld showed a much lower dislocation density and a more planar-like organisation similar to that of the base metal microstructure (Fig. 4). Both hardness measurements and microstructural observations are consistent with those reported in [21]. Thermal cycles and mechanical constraints during welding induce plastic strain in the weld-affected zone. Away from the fusion line, the base metal is unaffected, as the thermal gradient is accommodated by elastic deformation only. Getting closer to the fusion line, the more severe the thermal gradient experienced during welding, the higher the amount of plastic strain and hardness. Even closer, welding temperature peaks become high enough (around 700 °C) to partially recover the dislocation microstructure; consequently, hardness reaches a maximum and finally decreases approaching the fusion line. More detailed analysis of thermal–mechanical cycles in the weld-affected zone is reported in [22]. Both intergranular and intragranular $M_{23}C_6$ carbides nucleated at dislocations were observed in the weld-affected zone as well as in the base metal (Fig. 4). Sigma and Laves phases were also noticed in ferrite stringers. These microstructural features are consistent with ageing duration and precipitation kinetics as reported in literature [23]. The increase in hardness in the weld-affected zone could be partly due to these "strain-induced" intragranular carbides. However, the fact that unaged 316 weld-affected zones present similar hardening (see next section and [20]) suggests that the

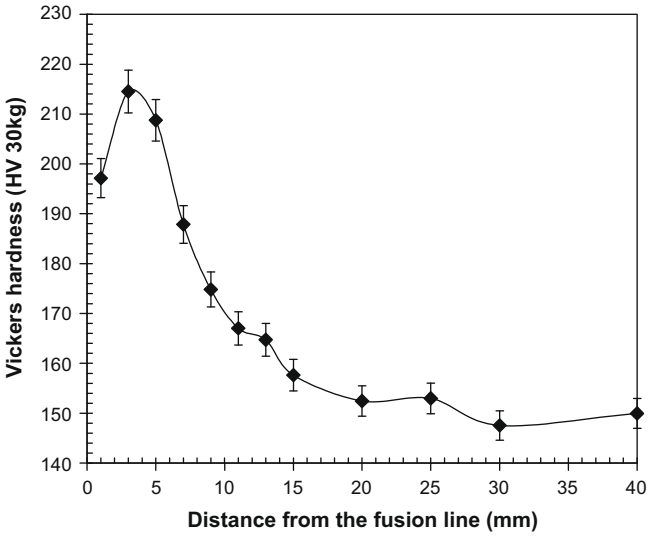


**Fig. 2.** Vickers hardness under 30 kg near an uncracked as-received weld in 316H.

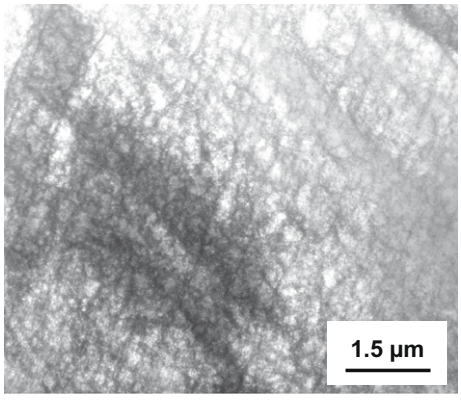


**Fig. 3.** Dislocation microstructure of as-received weld-affected zone of 316H, 0.2 mm away from the fusion line (bright-field TEM imaging).

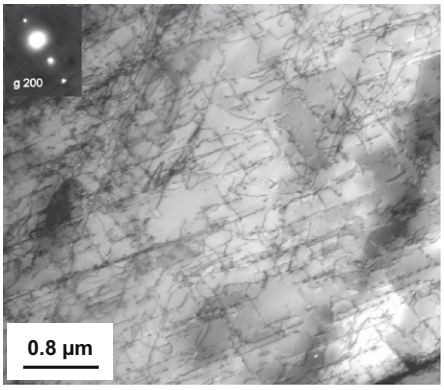


**Fig. 4.** Dislocation microstructure of as-received 316H base metal (bright-field TEM imaging).

increase in dislocation density could be the major cause of hardening in the investigated 316H welds.

*3.1.2. Unaged 316L(N) weld-affected zone*

In order to evaluate the influence of welding parameters on residual strains in the weld-affected zone, two welds were realised on grooved 30-mm-thick 316L(N) plates using an automatic tungsten inert gas (TIG) technique. One groove was filled using two passes and another one using four passes. Welding passes did not overlap over the full length of the weld, so that polished cross-sections could be taken after each pass. The weld torch travel rate was 40 mm/min and the heat input energy was 2 kJ/mm for each pass. The Vickers hardness under 10 kg was measured with a step size of 2 mm on polished cross-sections after each welding pass. The geometry of the welds is indicated together with hardness maps in Figs. 5 and 6. Concerning the weld performed in two passes (Fig. 5), the hardness in the weld-affected zone was higher after the second pass than after the first one. Concerning the weld performed in four passes, the hardness in the weld-affected zone was even higher (Fig. 6). These results reveal the cumulative increase in plastic strain and hardness due to welding passes. The increase in the X-ray peak width with the number of passes (Fig. 7) also confirmed this effect. Other authors [24–26] determined the amount of strain in an AISI 316 weld-affected zone using electron backscatter diffraction. They also found considerable increase in residual strain (up to 20%) over the first 5 mm from the fusion line.

*3.2. Characterisation of pre-strained materials*

As shown in the previous section, the typical size of the weld-affected zone does not allow extraction of specimens for conventional mechanical testing. Thus, it was decided to modify the base metal microstructure to simulate the weld-affected zone on much larger volumes. In order to reproduce the microstructure of the hardest part of unaged weld-affected zones, annealed plates of base metal materials (see Section 1) were pre-strained by warm rolling between 400 °C and 600 °C. Using following thickness reduction ratios 15 ± 0.4% for 316L(N) and 316H and 17.5 ± 0.4% for 316L, similar hardness (~230 $HV_{30}$) was obtained for all three pre-strained steels (Table 2). As subsequent mechanical testing (see Section 4) was performed at 600 °C, characterisation was also performed on pre-strained, then aged materials. Table 2 indicates that pre-strain hardening can be partially reduced by thermal ageing: slightly for 316H and 316L(N) and more significantly for 316L.

The dislocation microstructure of unaged but pre-strained 316H samples is presented in Fig. 8. High dislocation density and cell organisation similar to those of the actual weld-affected zone (Fig. 3) are noticeable. No carbide was observed, which indicates that annealing performed before pre-strain completely dissolved carbides precipitated during ageing and that pre-straining between 400 °C and 600 °C was quick enough not to precipitate carbides. Good agreement between the microstructure of 316L(N) unaged weld-affected zone and the microstructure of 316L(N) pre-strained samples was reported earlier [20]. TEM examination of a sample of 316H steel pre-strained, then aged for 200 h at 600 °C revealed intergranular and intragranular carbides (nucleated at dislocations), whereas only intergranular carbides could be detected in a sample of 316L(N) steel that was pre-strained, then aged for 500 h at 600 °C. This result is consistent with literature data

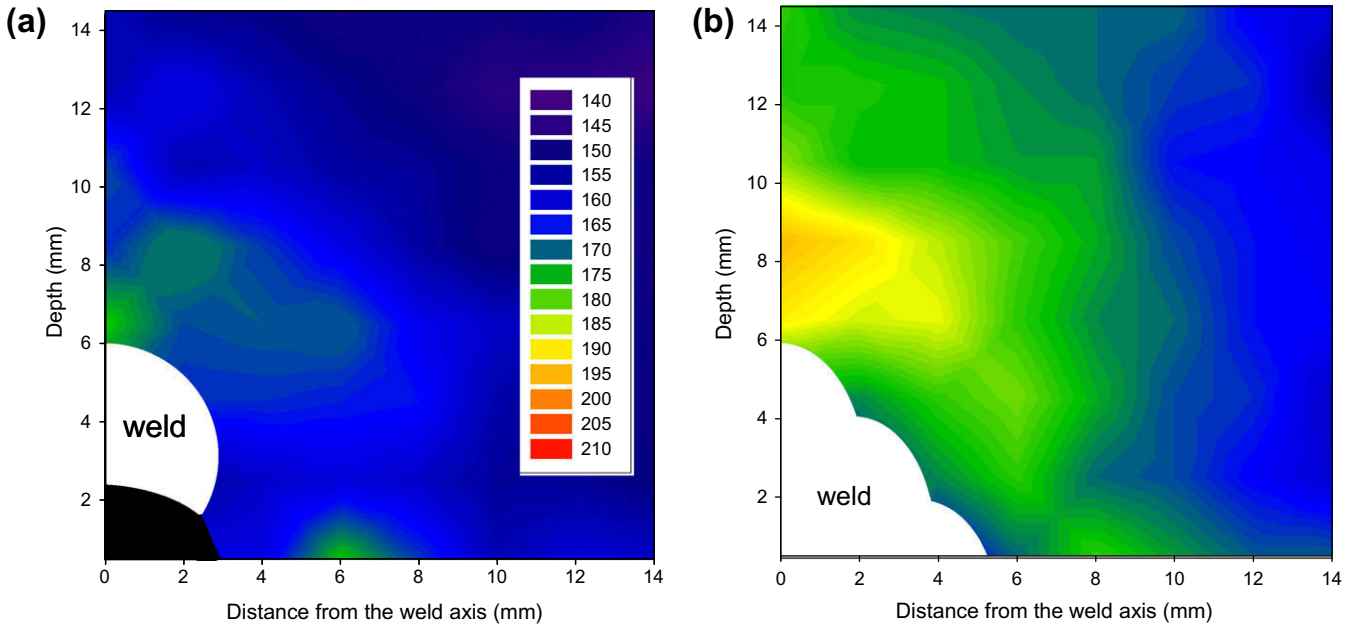


**Fig. 5.** Vickers hardness under 10 kg of 316L(N) unaged TIG weld performed in two passes, (a) after the first pass and (b) after the second pass. Weld passes are schematically indicated at the bottom left corner.

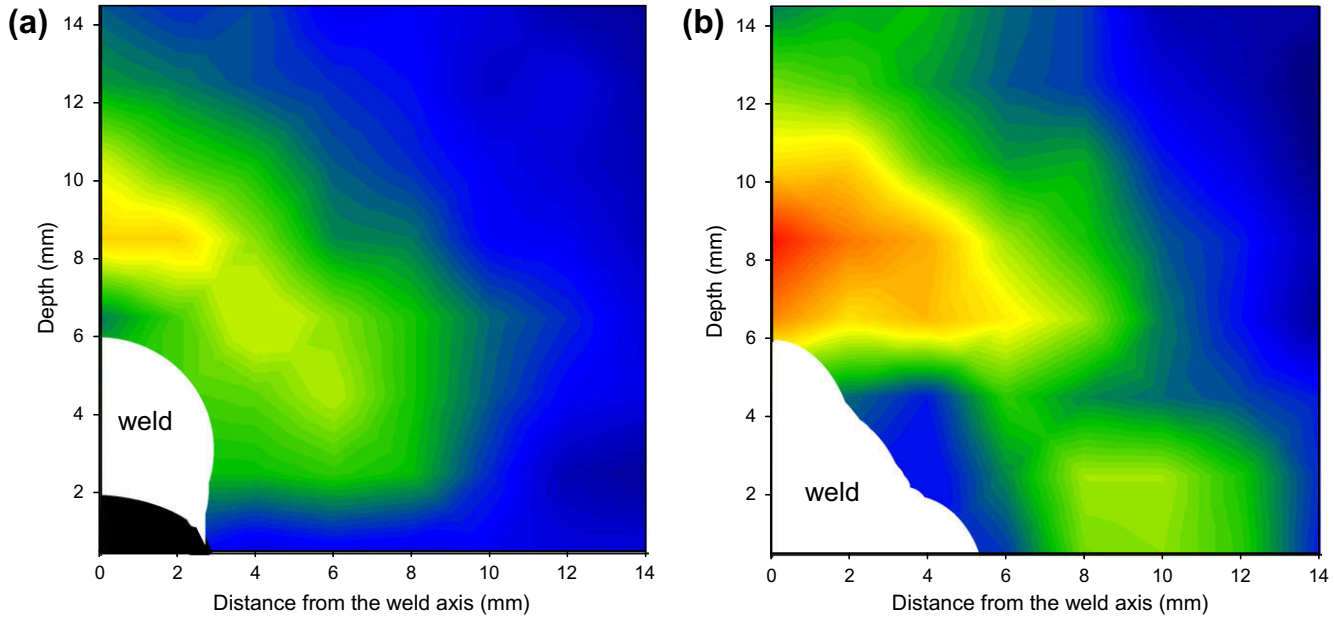


**Fig. 6.** Vickers hardness under 10 kg of 316L(N) unaged TIG welds performed in four passes, (a) after the second pass and (b) after the fourth pass, same scale as Fig. 5. Weld passes are schematically indicated at the bottom left corner.

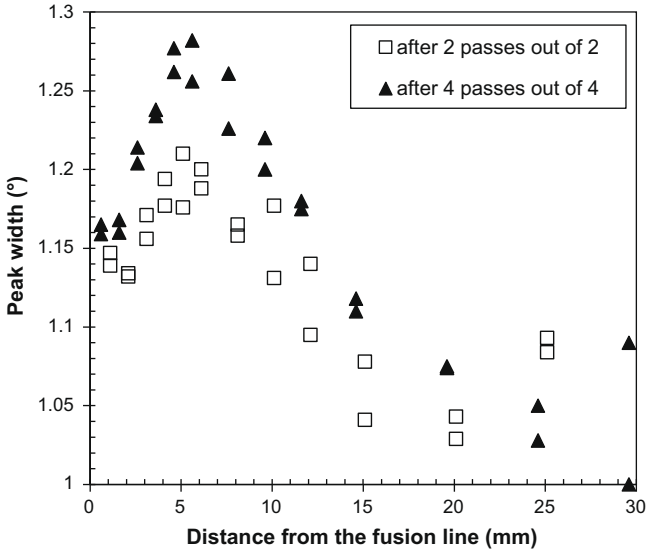


**Fig. 7.** {3 1 1} X-ray diffraction peak width of 316L(N) unaged TIG welds performed in two and four passes.

**Table 2**
Mean Vickers hardness under 30 kg of the three studied steels in as-received, annealed and pre-strained (unaged or aged) states.

| | 316L(N) | 316H | 316L |
|---|---|---|---|
| As-received | 149 | 149 | 132 |
| Annealed | 135 | 131 | 132 |
| Pre-strained | 227 | 232 | 230 |
| Pre-strained then aged for 2 h at 600 °C | 227 | 221 | 211 |
| Pre-strained then aged for 24 h at 600 °C | 222 | 219 | 198 |
| Pre-strained then aged for 2 h at 700 °C | 208 | 201 | 183 |
| Pre-strained then aged for 24 h at 700 °C | 207 | 201 | 180 |

indicating a strong effect of carbon content on the carbide precipitation kinetics [27].

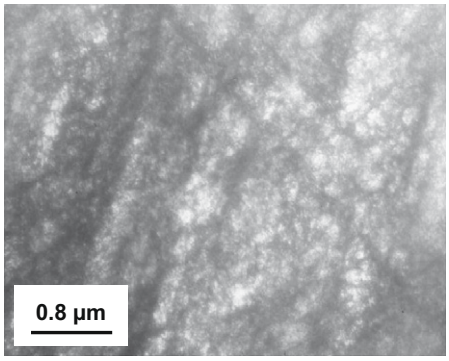


**Fig. 8.** Dislocation microstructure of pre-strained 316H (bright-field TEM imaging).

## 4. Mechanical tests

### 4.1. Deformation of smooth specimens

#### 4.1.1. Tensile tests

Results of uniaxial tensile tests at 600 °C are reported in Table 3. Results on the three steels are not significantly different. As reported in [20] for 316L(N), pre-straining drastically increased the yield strength of 316H stainless steel and decreased its residual strain hardening capacity. Both annealed and pre-strained stainless steels exhibited dynamic strain-ageing (DSA) for strain rates between $10^{-4}$ and $10^{-3}$ $s^{-1}$, whereas no significant strain rate sensitivity could be detected. These results are in accordance with literature data concerning DSA of 316 type stainless steels [28,29] and suggest that solute drag is the major solute–dislocation interaction mechanism for strain rates lower than $10^{-4}$ $s^{-1}$ at 600 °C. Hardness measurements (Table 2) as well as comparison between two tensile tests performed on pre-strained 316L – the first one started immediately after reaching 600 °C, the second one started after additional soaking for 2 h at 600 °C – confirmed that recovery is ongoing for this steel at this temperature.

**Table 3**
Results of tensile tests performed at 600 °C on smooth specimens of the three studied steels in annealed and pre-strained states.

| Material | State | Strain rate ($s^{-1}$) | Uniform elongation (%) | 0.2% Yield stress (MPa) | Tensile strength (MPa) |
|---|---|---|---|---|---|
| 316L(N) | Annealed | $1 \times 10^{-3}$ | 36 | 118 | 406 |
| 316L(N) | Annealed | $1 \times 10^{-4}$ | 34 | 122 | 394 |
| 316L(N) | Annealed | $5 \times 10^{-5}$ | 27 | 105 | 357 |
| 316L(N) | Pre-strained | $5 \times 10^{-4}$ | 6 | 418 | 466 |
| 316L(N) | Pre-strained | $1 \times 10^{-5}$ | 2 | 378 | 444 |
| 316H | Annealed | $1 \times 10^{-3}$ | 37 | 134 | 393 |
| 316H | Annealed | $1 \times 10^{-4}$ | 37 | 134 | 386 |
| 316H | Annealed | $3 \times 10^{-5}$ | 26 | 128 | 369 |
| 316H | Pre-strained | $1 \times 10^{-4}$ | 5 | 398 | 432 |
| 316H | Pre-strained | $1 \times 10^{-3}$ | 8 | 388 | 448 |
| 316H | Pre-strained | $3 \times 10^{-5}$ | 5 | 361 | 438 |
| 316L | Pre-strained | $5 \times 10^{-4}$ | 9 | 373 | 442 |
| 316L | Pre-strained then aged 2 h at 600 °C | $5 \times 10^{-4}$ | 7 | 346 | 416 |

#### 4.1.2. Creep tests

As described in [20] for 316L(N), creep tests on 316H and 316L revealed marked differences between annealed and pre-strained materials. Plastic deformation during loading occurred only for the annealed material (plastic loading strains between 6.5% and 12% and between 2.5% and 8% were recorded for 316H and 316L, respectively) because of the difference in yield stress between annealed and pre-strained materials. However, the amount of strain applied during creep loading of annealed materials remains much smaller than that applied during warm rolling of pre-strained materials. The amount of primary creep strain was also reduced by pre-strain: it was found higher than 1.5% for annealed materials, whereas it remained lower than 0.5% for pre-strained materials. As illustrated in Fig. 9, pre-strain caused a decrease in the minimum creep rate by two orders of magnitude for the three studied steels. Such a significant effect of pre-strain on the creep strain rate was already observed for cold worked type 316L(N) at 675 °C [30] and type 316H at 575 °C [31] and 600 °C [32]. As similar pre-strain hardening was obtained for the three studied steels regardless their differences in intragranular precipitation state, the increase in dislocation density should therefore be the major cause of pre-strain hardening. Ajaja and Ardell [33] correlated the creep rate at 677 °C with the dislocation density as a function of cold-work level of a type 304 stainless steel and proposed the same interpretation. Fig. 9 also indicates that annealed 316L showed significantly lower creep resistance than annealed 316L(N), which illustrates the well-known hardening role of the nitrogen solute content. Comparison between creep properties of annealed type 316L(N) and type 316H steels at 600 °C has already been done by Mathew et al. [34]. They found type 316L(N) to be slightly more creep resistant, in particular for long-term creep tests. A similar tendency was noticed in the present study for longer-term tests, whereas 316H appeared slightly more creep resistant for shorter-term tests. As intragranular carbides only precipitate in 316H, these results suggest that strengthening by intragranular carbide precipitation did not compensate the loss of solute carbon strengthening associated to this precipitation during longer-term tests. Fig. 9 also shows that pre-straining did not modify the effect of carbon and nitrogen content on the creep rate: (i) pre-strained 316L was found to be significantly less creep resistant than pre-strained 316H and 316L(N) and (ii) 316H was slightly less creep resistant than 316L(N) concerning long-term creep tests.

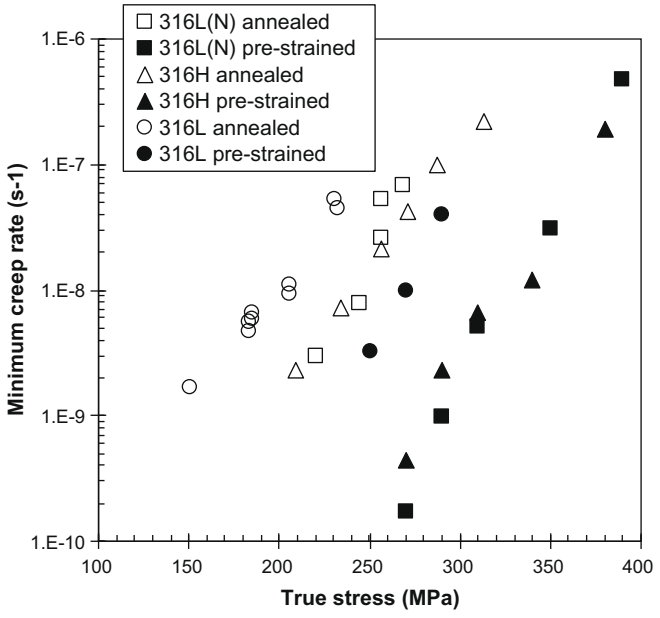


**Fig. 9.** Minimum creep strain rate at 600 °C versus true stress for 316L(N), 316H and 316L uniaxial specimens, the true stress is calculated from the engineering stress right after the loading stage of the test.

### 4.2. Fracture of smooth specimens

Average and minimum values of fracture elongation and reduction of area of smooth specimens used for tensile and creep tests are displayed in Table 4. Regarding tensile tests, no significant difference between the three studied steels was observed. Pre-strain caused a significant decrease in fracture elongation, but the reduction in area (and thus, the intrinsic ductility of the material at high strain rates) remained high. Regarding creep tests, measurements on 316L(N) and 316L yielded similar values but 316H was found significantly less ductile. Creep fracture elongation as low as 0.9% was measured (see Table 4) for pre-strained 316H. Pre-strain also caused a drop of both fracture elongation and reduction of area of crept specimens. Moreover, a significant decrease in ductility with decreasing the strain rate (from tensile tests to creep tests) was observed for both annealed and pre-strained materials. These results will be discussed in Section 6 in relation to the fracture surface analysis.

Table 4 also presents the Monkman–Grant product (minimum creep strain rate multiplied by creep lifetime [35]). As expected, this product was fairly constant for a given material in a given metallurgical state. However, pre-strain decreased it by almost a factor of 10. For a given creep stress, pre-straining increased time to fracture but not as much as it decreased the minimum creep strain rate because of a loss in ductility. Pre-strain was also found to decrease the amount of strain at the onset of tertiary creep stage (lower than 1% for pre-strained materials). Similar results were found by Wilshire and Willis on cold worked 316H [31].

**Table 4**
Minimum and mean fracture elongation and reduction in area for tensile and creep tests performed at 600 °C on smooth specimens of the three studied steels in annealed and pre-strained states, the Monkman–Grant product is defined as the minimum creep rate (%/h) multiplied by the time to fracture (h).

| | Tensile tests | | | Creep tests | | | |
|---|---|---|---|---|---|---|---|
| | Fracture elongation (%) | | Reduction in area (%) | Fracture elongation (%) | | Reduction in area (%) | Monkman–Grant product (%) |
| | Min. values | Mean values | Mean values | Min. values | Mean values | Mean values | Mean values |
| 316L(N), annealed | 49 | 52 | 56 | 23 | 34 | 48 | 10.1 |
| 316L(N), pre-strained | 22 | 25 | 62 | 6 | 10 | 30 | 1.6 |
| 316H, annealed | 33 | 49 | 56 | 13 | 18 | 23 | 4.4 |
| 316H, pre-strained | 21 | 22 | 47 | 0.9 | 3 | 13 | 0.6 |
| 316L, annealed | Not determined | | Not determined | 37 | 41 | 49 | 10.2 |
| 316L, pre-strained | 20 | 24 | 56 | 8 | 9 | 25 | 1.8 |

Relaxation of residual stresses in the vicinity of welds only requires a small amount of creep strain (~0.2%). Even pre-strained 316H – the most brittle stainless steel studied here – should therefore sustain this strain without cracking. However, creep ductility is known to decrease drastically when stress triaxiality increases [11–17]. In order to assess the reheat-cracking sensitivity of the studied materials with more realistic mechanical loading conditions, dedicated mechanical tests with high local stress triaxiality were therefore carried out. The results are described in the next section.

### 4.3. Relaxation tests on CT specimens

Initial load levels on pre-cracked CT specimens were chosen between the elasticity limit load of annealed materials and the one of pre-strained materials, so that load-opening curves were always linear for pre-strained materials but not for annealed ones. The extent of crack propagation, which occurred during these relaxation tests is given in Table 5. As expected, pre-strain clearly enhances sensitivity to cracking in these conditions. Tests on annealed materials did not lead to crack propagation over more than 0.5 mm, whereas several millimetre long cracks were observed on pre-strained materials. Table 5 also reveals that pre-strained 316L was the most sensitive to relaxation cracking: in this material, with $K_{initial}$ = 42 MPa $\sqrt{m}$, a 9.8-mm-long crack was observed after 200 h at 600 °C, but only a 7.3-mm-long crack in pre-strained 316H and a 2.4-mm-long crack in pre-strained 316L(N) after 600 h. Fig. 10 indicates that, for a given test duration, the extent of crack propagation decreased with decreasing $K_{initial}$. However, no threshold stress intensity factor was clearly identified, even low values of the initial stress intensity factor led to crack propagation. A few relaxation tests on CT specimens after pre-straining and a short ageing for 2 h at 700 °C have also been performed (Table 5). As expected, ageing after pre-straining reduced the extent of crack propagation – particularly concerning 316L, which is consistent with the decrease in hardness measured after ageing (Table 2). However, this ageing effect was not sufficient to avoid relaxation crack propagation.

## 5. Fracture surface observations

Observation by SEM of the fracture surfaces of smooth specimens revealed a similar damage mechanism for 316L(N), 316H and 316L in annealed and pre-strained states. Nevertheless, a marked difference in damage and fracture mechanisms occurring

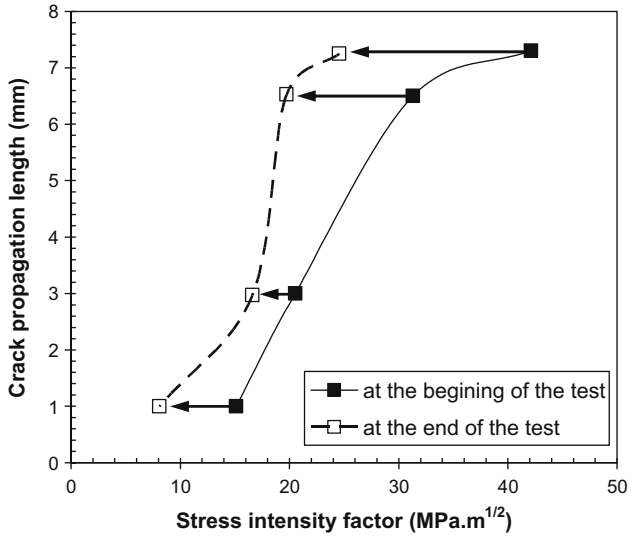


**Fig. 10.** Crack propagation length during relaxation for 600 h at 600 °C on pre-strained 316H pre-cracked CT specimens versus the stress intensity factor, which is calculated both at the beginning and at the end of the test.

**Table 5**
Results of relaxation tests at 600 °C on pre-cracked CT specimens.

| Material | State | $a_0/W$ | Initial stress intensity factor (MPa $\sqrt{m}$) | Final stress intensity factor (MPa $\sqrt{m}$) | Opening (μm) | Test duration (h) | Crack propagation length (mm) |
|---|---|---|---|---|---|---|---|
| 316L(N) | Annealed | 0.499 | 25 | 15 | 248 | 1004 | 0.0 |
| 316L(N) | Annealed | 0.501 | 31 | 18 | 578 | 1006 | 0.0 |
| 316L(N) | Pre-strained | 0.494 | 41 | 22 | 214 | 619 | 2.4 |
| 316L(N) | Pre-strained | 0.493 | 30 | 18 | 136 | 608 | 1.5 |
| 316L(N) | Pre-strained then aged 2 h at 700 °C | 0.503 | 42 | 30 | 231 | 652 | 1.8 |
| 316H | Annealed | 0.503 | 31 | 23 | 803 | 652 | 0.5 |
| 316H | Pre-strained | 0.494 | 41 | 27 | 200 | 571 | 7.3 |
| 316H | Pre-strained | 0.490 | 30 | 21 | 114 | 577 | 6.5 |
| 316H | Pre-strained | 0.496 | 20 | 18 | 116 | 598 | 3.0 |
| 316H | Pre-strained | 0.491 | 15 | 9 | 68 | 597 | 1.0 |
| 316L | Pre-strained | 0.500 | 42 | 28 | 291 | 206 | 9.8 |
| 316L | Pre-strained then aged 2 h at 700 °C | 0.498 | 42 | 35 | 201 | 205 | 2.8 |

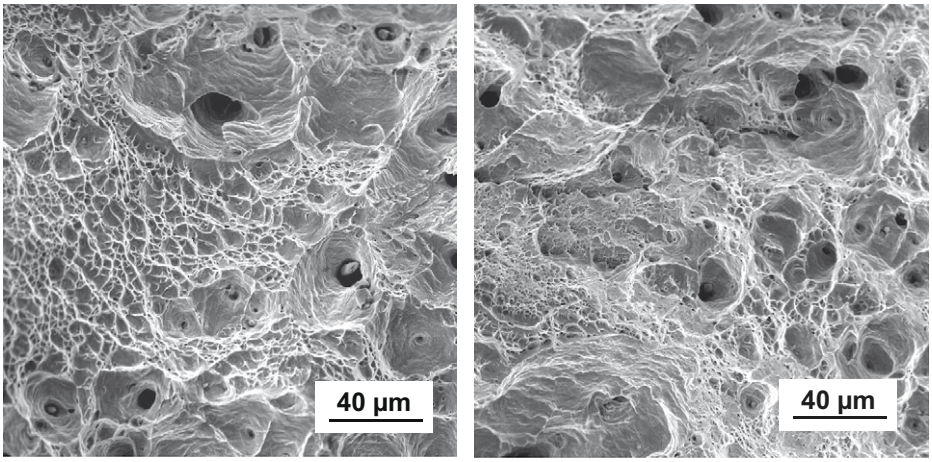


**Fig. 11.** Fracture surfaces of annealed and pre-strained 316H smooth specimens after tensile testing at 600 °C (secondary electron SEM images).

during tensile tests and creep tests was noticed. On the one hand, SEM pictures of fracture surfaces of tensile tested specimens revealed dimples nucleated at inclusions and ferrite stringers (Fig. 11). Polished longitudinal sections observed with an optical microscope confirmed that the damage mode was transgranular ductile cavity nucleation, growth and coalescence initiating at the centre of the specimens and finally transgranular ductile shear of the remaining annular ligament ("cup and cone" fracture). On the other hand, the fracture surfaces of creep tested specimens were partially intergranular (Fig. 12) and partially transgranular. Observation of polished longitudinal cross-sections of un-fractured specimens proved that intergranular damage developed progressively during creep by nucleation, growth and linkage of intergranular cavities (similarly to reheat-cracking damage), whereas transgranular ductile damage only developed at the very end of the test. This well-known transition in damage mode with the strain rate is due to the competition between (visco)plastic flow, which drives ductile damage, and grain boundary diffusion, which plays a role in intergranular damage development [36,37]. The drop of ductility from tensile to creep tests observed for the three studied steels (see Section 4.2) is obviously linked to this transition in damage mode.

For a given strain rate, no qualitative difference in damage and fracture mode was found between annealed and pre-strained specimens (Figs. 11 and 12), although pre-strain did reduce fracture elongation (Table 4). In the upper range of strain rate (i.e., for tensile tests), reduction of both uniform elongation and fracture elongation by pre-strain surely resulted from the reduction of residual work hardening capacity, which enhanced plastic instability and strain localisation before fracture. In the lower strain rate range (i.e., for creep tests), the reduction of fracture elongation most probably resulted from the enhancement of intergranular damage by pre-strain, as already described in [20] for 316L(N), which will be discussed in Section 6.

Although creep testing revealed that 316H was more brittle than 316L(N) and 316L, both in annealed and pre-strained states (Table 4), no difference in damage mode between the three steels was noticed from fracture surface observations. The relative brittleness of the 316H steel could be due to its higher grain size (150 µm) because creep ductility is known to decrease when the grain size increases in the range 25–400 µm [38]. It could also result from different intergranular carbide morphology or different intergranular impurity segregation (such as sulphur or boron for example) – two parameters also known to affect creep ductility [39–42].

Crack propagation during relaxation tests of pre-cracked CT specimens was always fully intergranular (Fig. 13a). Where the oxide layer was not too thick on the fracture surfaces,

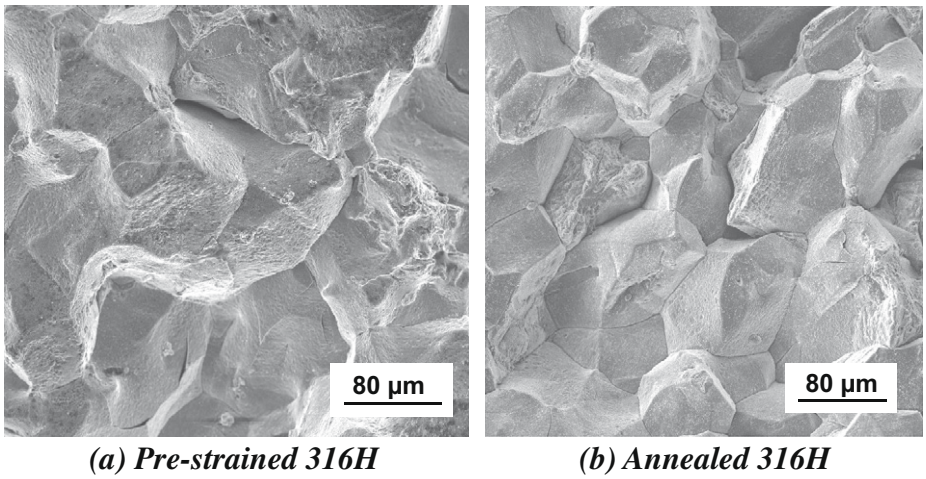


**Fig. 12.** Fracture surface after creep testing at 600 °C of annealed and pre-strained 316H smooth specimens (secondary electron SEM images).

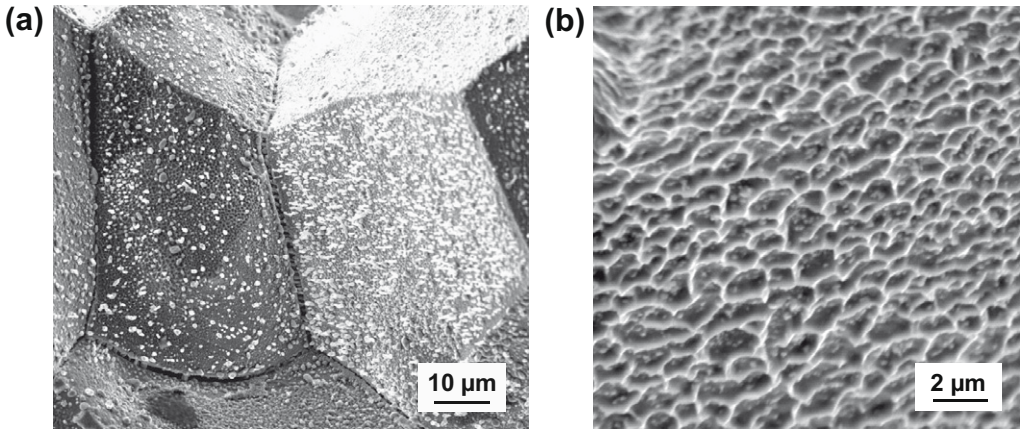


**Fig. 13.** Fracture surfaces after relaxation at 600 °C of pre-strained 316H pre-cracked CT specimens (secondary electron SEM images), (a) relatively low magnification image of intergranular facets, (b) higher magnification image showing micro-dimples on an intergranular facet.

micro-dimples around carbides were noticed on intergranular facets (Fig. 13b). The fracture mechanism was therefore similar to that observed for actual (in-service) reheat cracks.

## 6. Discussion

### 6.1. Effect of solute atoms on creep and reheat cracking

One of the goals of the present study was to evaluate the effect of carbon and nitrogen content of type 316 austenitic stainless steels on creep and reheat cracking behaviour. The difference in creep flow and kinetics of dislocation recovery after pre-strain of 316L to those of 316L(N) and 316H evidences the strong strengthening role of solute carbon and nitrogen at 600 °C. On the other hand, creep and hardness results for 316L(N) and 316H steels indicated that strain-induced carbide precipitation – which only occurred in 316H in the studied conditions – was slightly less efficient than solute atom strengthening.

Regarding the effect of carbon and nitrogen on reheat cracking, two different mechanisms were proposed in the literature for stabilised stainless steels. The first one [1–4] relies on strain-induced precipitation hardening, the second one on solute–dislocation hardening.

Transposition of the first mechanism to the unstabilised 316 stainless steels leads to the assumption that 316L(N) and 316L should not be sensitive to reheat cracking. However, relaxation tests on CT specimens revealed crack propagation for both of these steels in the pre-strained state. Consequently, in accordance with Chabaud-Reytier et al. who worked on a stabilised stainless steel [10], the present study showed that strain-induced precipitation is not a key parameter for reheat cracking of type 316 stainless steels.

Transposition of the second mechanism to unstabilised 316 stainless steels leads to the assumption that a low solute atom content (such as in 316L) should be beneficial to reheat cracking resistance. Surprisingly, present results showed that 316L was more sensitive to relaxation crack propagation than 316H and 316L(N). Consequently, carbon and nitrogen content seems to play a minor role in reheat cracking of type 316 stainless steels. On the contrary, in accordance with the work of Chabaud-Reytier et al. on stabilised stainless steel [10], present results enlighten the major importance of pre-strain and stress triaxiality in the sensitivity to reheat cracking.

Although no industrial occurrence of reheat cracking in type 316L stainless steel has been reported so far, a low solute content should not be considered as sufficient to avoid reheat cracking of austenitic stainless steels. Nevertheless, as a low solute content increases the recovery kinetics of the dislocation network introduced by pre-strain, post-weld heat treatments avoiding the reheat cracking risk should be easier to define on 316L than on 316H and 316L(N). Tests on CT specimens pre-strained and then aged for 2 h at 700 °C were performed following this idea. Unfortunately, this ageing treatment was not sufficient to avoid relaxation crack propagation.

### 6.2. Effect of pre-strain on creep and reheat cracking

Whatever the solute content, pre-straining was found to significantly decrease creep ductility for a given strain rate. Fracture surface observations revealed that this effect was not due to a change in damage mechanism but to an enhancement of intergranular damage development. Reduced creep ductility due to pre-strain combined with high stress triaxiality was found to cause relaxation cracking in CT specimens. In the present section, an attempt is made to give insight into the mechanism by which pre-strain influences creep ductility.

In the present study, intergranular damage development occurred by nucleation and growth of intergranular cavities. Several cavity growth mechanisms have been described in literature (see reviews by Kassner and Riedel [36,37]). However, for a given value of strain rate and stress triaxiality, growth rate formulae proposed in literature are not sensitive to pre-strain. Concerning cavity nucleation, literature models [36,37] underline that it requires high local stress, which is consistent with the fact that intergranular cavities are frequently observed at triple junctions, around intergranular particles and at boundaries oriented perpendicular to the direction of maximum principal stress. Although the global (macroscopic) strain does not appear as a parameter *per se* in physical modelling of intergranular cavity nucleation, numerous studies reported continuous nucleation of intergranular cavities with increasing creep strain [43,44]. Consequently, enhancement of creep damage by pre-strain seems to be linked to cavity nucleation rather than to cavity growth.

From the present authors' point of view, the heterogeneous nature of plastic deformation in polycrystals leads to high local stresses at grain boundaries, which increases the cavity nucleation rate. Indeed, due to different crystallographic orientations, neighbouring grains experience different strain levels, which cause deformation incompatibilities and intergranular over-stresses. Diard et al. [45] for example, using finite element computations of 3D multicrystalline aggregates, showed that the magnitude of these over-stresses increases with average strain. Moreover, intragranular

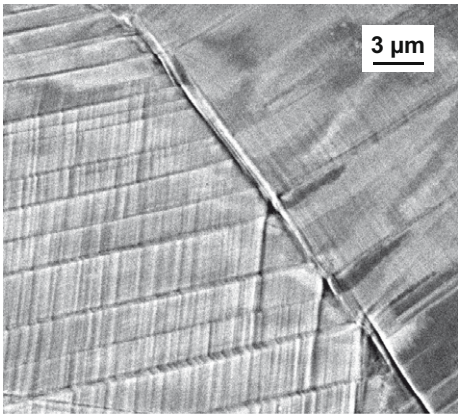


**Fig. 14.** Back-scattered electron SEM image of a flat specimen of annealed 316L(N), which was polished, then 4% strained in tension at 600 °C in vacuum.

strain localisation into slip bands should lead to even higher local stress concentrations. Fig. 14 illustrates such slip bands, which developed at the surface of an annealed 316L(N) flat specimen during plastic tensile strain of approximately 4% at 600 °C in vacuum. Skelton et al. [12] reported similar slip bands and grain boundary steps developed during mock-up welding thermo-mechanical cycles. The lower the stacking fault energy, the more planar the dislocation distribution and the higher the local stress concentration. Consequently, low stacking fault energy f.c.c. alloys are expected to be more sensitive to pre-strain induced over-stresses than high stacking fault energy f.c.c. alloys.

The pre-strain effect responsible for the reheat-cracking sensitivity of austenitic stainless steels could therefore have the same origin as the pre-strain effect on Nimonic 80 nickel base alloy described by Dyson et al. [46–48]. This mechanism is also consistent with the occurrence of reheat cracking on un-welded, but cold-worked components [8]. In such a mechanism, the solute content does not play a significant role, which is consistent with the fact that all three studied stainless steels presented an effect of pre-strain on creep ductility and relaxation cracking sensitivity in the pre-strained state.

### 6.3. Reheat cracking risk assessment

Following Dhooge's review on reheat cracking [8], key parameters for reheat cracking are thickness, notches and weld defects, grain size, hardness and strain-induced precipitation. Thickness, notches and weld defects are deleterious because ductility sharply decreases as stress triaxiality increases [11–17]. Following the results of the present study, thickness has an additional effect: welding thick components requires numerous welding passes which leads to a high level of pre-strain in the weld-affected zone, which impairs ductility. A coarse grain size is also deleterious because it decreases creep ductility [38]. Hardness, from the present authors' point of view, is a convenient indicator of the level of pre-strain or of the extent of dislocation network recovery of unstabilised austenitic stainless steels, but is not a reliable way to assess the reheat cracking susceptibility: For example, after pre-straining and ageing for 2 h at 700 °C, 316L was much softer than the 316L(N), (180 HV and 210 HV respectively) but tests on CT specimens proved it was still more sensitive to relaxation cracking than the 316L(N) steel.

In order to assess the reheat cracking risk or to help designing safe post-weld heat treatments of 316H stainless steel, several authors [49,50] estimated residual stresses by thermal–mechanical finite element calculations and used Spindler's multi-axial damage model [13,14] to quantify intergranular crack development during stress relaxation. This method has proved its efficiency (see [16,17] for example). However, the present study illustrated the significant effect of welding-induced pre-strain on both creep flow and creep ductility, which are not explicitly taken into account in such a method. On the other hand, constitutive equations and intergranular damage model developed in [11] for 316L(N) take these effects into account but have not been validated yet on real reheat cracked welds.

## 7. Conclusions

Multi-pass welding-induced pre-strain which considerably increased the hardness and decreased the creep rate at 600 °C of type 316 stainless steels by increasing the dislocation density, independently from the carbon and nitrogen contents.

The low ductility of the weld-affected zone leading to reheat cracking of 316 stainless steels is due to the combined effect of both welding-induced pre-strain and stress triaxiality. High solute content and strain-induced carbide precipitation, which are thought to increase the reheat cracking risk of stabilised austenitic stainless steels, did not appear as key parameters in reheat cracking of 316 stainless steels. Consequently, although no industrial occurrence of reheat cracking in type 316L stainless steel has been reported so far, 316L should not be a priori considered as immune.

The deleterious effect of pre-strain on creep ductility is not due to a change in damage mechanism but to an enhancement of intergranular damage development. The intergranular creep cavity nucleation rate could be increased by high intergranular stresses, generated by the heterogeneous nature of plastic deformation in pre-strained f.c.c. polycrystals with relatively low stacking fault energy.

## Acknowledgements

The authors would like to thank M.W. Spindler from British Energy for providing 316H material and P. Todeschini from EDF for X-ray diffraction analysis of 316L(N) welds. Following CEA participants are also acknowledged: D. Ayrault and O. Blanchot for 316L(N) weld study, I. Tournié, B. Girard and E. Héripré for performing uniaxial tensile and creep tests and T. van den Berghe for TEM examinations.

## References

[1] R.M. Curran, A.W. Rankin, Trans. ASME (August) (1957) 1398–1409.
[2] R.W. Emerson, R.W. Jackson, Res. Suppl. Weld. J. (February) (1957) 89–104.
[3] R.N. Younger, R.G. Backer, J. Iron Steel Inst. (October) (1960) 188–194.
[4] R.N. Younger, D.M. Haddrill, R.G. Backer, J. Iron Steel Inst. (August) (1963) 693–698.
[5] C.F. Meitzner, Weld. Res. Counc. Bull. 211 (1975) 1–17.
[6] R.D. Thomas, Weld. J. (December) (1984) 24–32 (Weld. J. (Suppl., December) (1984) 355–368).
[7] M.C. Coleman, D.A. Miller, R.A. Stevens, Reheat cracking and strategies to assure integrity of type 316 welded components, in: Integrity of High-temperature Welds, International Conference, Nottingham, 1998, November, Professional Engineering Pub., Bury St. Edmunds, 1998, pp. 169–179.
[8] A. Dhooge, Weld. World 41 (1998) 206–219.
[9] Ch. Cavagna, O. Gastaldi, L. Martin, V. Grabon, Nucl. Technol. 153 (2006) 274–281.
[10] M. Chabaud-Reytier, L. Allais, C. Caës, P. Dubuisson, A. Pineau, J. Nucl. Mater. 323 (2003) 123–137.
[11] Q. Auzoux, L. Allais, C. Caës, B. Girard, I. Tournié, A.F. Gourgues, A. Pineau, Nucl. Eng. Des. 235 (2005) 2227–2245.
[12] R.P. Skelton, I.W. Goodall, G.A. Webster, M.W. Spindler, Int. J. Press. Vess. Pip. 80 (2003) 441–451.
[13] M.W. Spindler, Fatigue Fract. Eng. Mater. Struct. 27 (2004) 273–281.
[14] M.W. Spindler, Mater. High Temp. 21 (1) (2004) 47–52.
[15] I.W. Goodall, R.P. Skelton, Fatigue Fract. Eng. Mater. Struct. 27 (2004) 267–272.
[16] F. Vakili-Tahami, D.R. Hayhurst, Philos. Mag. 87 (28) (2007) 4383–4419.
[17] M. Turski, P.J. Bouchard, A. Steuwer, P.J. Withers, Acta Mater. 56 (2008) 3598–3612.

[18] P.J. Bouchard, P.J. Withers, S.A. McDonald, R.K. Heenan, Acta Mater. 52 (2004) 23–34.
[19] G. Casarini, W. Dumini, L. Villa, L. Lana, G. Rivolta, G. Merckling, High temperature damage of stainless alloys with formation of cracks that show the presence of a metallic phase surrounded by large amounts of oxides, in: Innovation Stainless Steel, Florence, Italy, October 1993, pp. 3.71–3.76.
[20] Q. Auzoux, L. Allais, A.F. Gourgues, A. Pineau, Reheat cracking in austenitic stainless steels, in: A. Neimitz, I.V. Rokach, D. Kocanda, K. Golos (Eds.), 14th European Conference on Fracture: Fracture Mechanics Beyond 2000, 8–13 September 2002, Cracow, Poland, vol. I, EMAS, pp. 137–144.
[21] C.F. Etienne, O. Van Rossum, F. Roode, Creep of welded joints in AISI 316, in: Engineering Aspects of Creep, International Conference, Sheffield, 15–19 September 1980, vol. 2, Institution of Mechanical Engineers, London, 1980, pp. 113–121.
[22] Q. Auzoux, Reheat Cracking of Austenitic Stainless Steels – Influence of Work Hardening on Intergranular Damage, Ph.D. Thesis, Ecole Nationale Supérieure des Mines de Paris, 2004 (in French). <http://pastel.paristech.org/bib/archive/00000659/> .
[23] B. Weiss, R. Stickler, Metall. Trans. 3 (1972) 851–866.
[24] T.M. Angeliu, P.L. Andresen, E. Hall, J.A. Sutliff, S. Sitzman, Strain and microstructure characterisation of austenitic stainless steel weld HAZ's [heat affected zones], Paper 00186, in: Proceedings of Corrosion 2000, 55th Annual Conference and Exposition, Orlando, Florida, USA, 26–31 March 2000, NACE International.
[25] P.L. Andresen, T.M. Angeliu, W.R. Catlin, L.M. Young, R.M. Horn, Effect of deformation on SCC [stress corrosion cracking] of unsensitized stainless steel, Paper 00203, in: Proceedings of Corrosion 2000, 55th Annual Conference and Exposition, Orlando, Florida, USA, 26–31 March 2000, NACE International.
[26] T.M. Angeliu, P.L. Andresen, E. Hall, J.A. Sutliff, S. Sitzman, R.M Horn, Intergranular stress corrosion cracking of unsensitized stainless steels in BWR environments, in: Ninth International Symposium on Environmental Degradation of Materials in Nuclear Power Systems-Water Reactors, Newport Beach, California, USA, 1–5 August 1999, Minerals Met. Mater. Soc., 1999, pp. 311–318.
[27] N. Parvathavarthini, R.K. Dayal, J. Nucl. Mater. 305 (2002) 209–219.
[28] J.T. Barnby, J. Iron Steel Inst. (1965) 392–397.
[29] K.P. Peng, K.W. Qian, W.Z. Chen, Mater. Sci. Eng., A 379 (1–2) (2004) 372–377.
[30] K.G. Samuel, K. Bhanu Sankara Rao, S.L. Mannan, V.M. Radhakrishnan, Trans. Indian Inst. Met. 49 (1996) 407–412.
[31] B. Wilshire, M.R. Willis, Metall. Mater. Trans. A 35A (2004) 563–571.
[32] B.F. Dyson, M.S. Loveday, Engineering Aspects of Creep, International Conference, Sheffield, 15–19 September 1980, vol. 1, Institution of Mechanical Engineers, London, 1980, pp. 61–66.
[33] O. Ajaja, A.J. Ardell, Scr. Metall. 11 (1977) 1089–1093.
[34] M.D. Mathew, G. Sasikala, K. Bhanu Sankara Rao, S.L. Mannan, Mater. Sci. Eng. A148 (1991) 253–260.
[35] F.C. Monkman, N.J. Grant, Proc. Am. Soc. Test. Mater. 56 (1956) 593–620.
[36] M.E. Kassner, T.A. Hayes, Int. J. Plast. 19 (10) (2003) 1715–1748.
[37] H. Riedel, Fracture at High Temperatures, Springer-Verlag, Heidelberg, 1987.
[38] D.G. Morris, Met. Sci. (1978) 20–29.
[39] D.G. Morris, D.R. Harries, Met. Sci. (1978) 532–541.
[40] F. Garofalo, R.W. Whitmore, W.F. Domis, F. von Gemmingen, Trans. Metall. Soc. AIME 221 (1961) 310–319.
[41] K. Laha, J. Kyono, S. Kishimoto, N. Shinya, Scr. Mater. 52 (2005) 675–678.
[42] C.L. White, R.A. Padgett, R.W. Swindeman, Scr. Metall. 15 (1981) 777–782.
[43] N.G. Needham, T. Gladman, Met. Sci. (February) (1980) 64–72.
[44] S.H. Goods, T.G. Nieh, Scr. Metall. 17 (1983) 23–30.
[45] O. Diard, S. Leclercq, G. Rousselier, G. Cailletaud, Int. J. Plast. 21 (2005) 691–722.
[46] B.F. Dyson, D.E. Henn, J. Microsc. 97 (1973) 165–170.
[47] B.F. Dyson, M.J. Rodgers, Met. Sci. 8 (1974) 261–266.
[48] B.F. Dyson, M.S. Loveday, M.J. Rodgers, Proc. Roy. Soc. Lond. A 349 (1976) 245–259.
[49] T.P.T. Soanes, W. Bell, A.J. Vibert, Int. J. Press. Vess. Pip. 82 (4) (2005) 311–318.
[50] R.J. Dennis, L.E. Easterbrook, N.A. Leggatt, Application of modern weld modelling techniques in the design of a ring weld reheat cracking test specimen, in: American Society of Mechanical Engineers, Proceedings of PVP 2005, July 17–21, Denver, Colorado USA, Pressure Vessels and Piping Division Conference, ASME, 2005, pp. 799–808.